US Belle II Project
Conceptual Design Report

Principal Investigators:

D. M. Asner[†], J. E. Fast, R. T. Kouzes, G. Tatishvili, L. S. Wood
Pacific Northwest National Laboratory, Richland, Washington 99352

A. J. Schwartz, K. Kinoshita
University of Cincinnati, Cincinnati, Ohio 45221-0011

T. E. Browder, K. Nishimura, S. Vahsen, G. Varner
University of Hawaii, Honolulu, Hawaii 96822

A. Vossen
Indiana University, Bloomington, Indiana 47408

T. Pedlar
Luther College, Decorah, Iowa 52101

V. Savinov
University of Pittsburgh, Pittsburgh, Pennsylvania 15260, USA

R. Godang
University of South Alabama, Mobile, Alabama 36688

L. Piilonen
Virginia Polytechnic Institute and State University, Blacksburg, Virginia 24061-0435

G. Bonvicini, D. Cinabro
Wayne State University, Detroit, Michigan 48202

March 9, 2012

[†]Contact:david.asner@pnnl.gov

Contents

1 Technical Description

1.1 SuperKEKB Commissioning Detector

1.1.1 US Role in a Background Commissioning Detector

1.1.2 Commissioning Detector Motivation

1.1.3 Accelerator Group Goals / Motivation

1.1.4 Commissioning Detector Description and US Contributions

1.1.5 Commissioning Detector Design and Simulation

2 micro-BEAST-TPCs simulation

In this section, Monte Carlo simulations studies of the micro-BEAST-TPCs are described. These studies were performed in order to design and optimize the micro-BEAST-TPCs to be able to distinguish the different beam-induced backgrounds (Touschek, Radiative Bhabha and Coulomb) by measuring the angular distributions of the nuclear recoils procured when neutrons scatter elastically off the nuclei of the gas-target.

These section is divided into three parts: the **simulation framework** is introduced, the **design optimization** and the neutron **detection efficiency** are presented.

2.1 Simulation framework

Our Monte Carlo study of micro-BEAST-TPC performance is based on two detector simulators: BASF2 and CYGNUS (our TPC-simulator). BASF2 and CYGNUS are both a full detector simulator based on GEANT4 but also on a Fast Monte Carlo or Full simulation for CYGNUS. Our Fast Monte Carlo is based on MAGBOLTZ. Our Full simulation is based on SRIM and GARFIELD. At the moment, both simulators are separated but we are currently working in combining the GEANT4 part of CYGNUS into BASF2.

2.1.1 Simulation strategy

A two steps simulation strategy is adopted to enhance the recoil number due to the low neutron cross section and also because GEANT4 is not simulating the electrons drift under the influence of an electric field.

- first step: BASF2 simulation of the different beam-induced backgrounds. This step is used to determine the types, origins, energy and angular distributions of the particles

passing through the micro-BEAST-TPCs ie the beam-induced particles background profiles.

- second step: beam-induced particles background profiles served as an event generator for CYGNUS

2.1.2 BASF2

BASF2 tracks particles due to the beam-induced background from the interaction points through various Belle2 detector components, taking into account their various interactions with detector materials. There are three types of beam-induced background: Radiative Bhabha (RBB), Coulomb and Touschek. These beam-induced backgrounds are producing mostly electromagnetic particles and neutrons. We are planning to produce beam-induced background simulation corresponding to phase 2 stage. Phase 1 stage can not be used to test the beam-induced background simulation at the designed luminosity so there is no interest to simulate this stage. All our studies are based on the 5th compaign of beam-induced background simulation produced by Nakayama-San at the designed luminosity and with the full Belle2 setup. The luminosity at the end of phase 2 should be 100 smaller than the one at designed luminosity. All rates originating from RBB, Touschek and Coulomb bacground presented below have been scaled by a factor 1/100. It should be noted only RBB background is scaling with luminosity. Touschek and Coulomb backgrounds are not scaling with the luminosity and only require one beam. Touschek background is scaling with the particles density per beam bunch. Coulomb or beam-gas bakcground is scaling with the Pressure. So in principal in phase 2, the Touschek and Coulomb background rates can be increased by the accelerator people by increasing respectively the beam bunch density and the pressure in the beam pipe.

2.1.3 TPC-simulator (CYGNUS)

The TPC-simulator aka CYGNUS is done in two steps:

- first step: beam-induced particles background profiles served as an event generator for the GEANT4 part of CYGNUS.
- second step: Fast Monte Carlo for
  - electron drift parameterization (using v_{drift}, D_l and D_t)
  - GEMs or avalanche-charge parameterization
  - digitization into pixel hit

Figure 2.1.3 shows a flow chart of CYGNUS. There is the possibility to use a full simulation for the electron drift and also to use SRIM transport model instead of SRIM-like GEANT4 transport model.

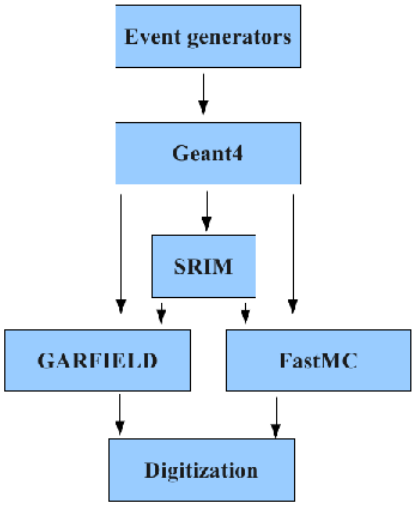

Figure 1: Flow chart showing the simulation steps.

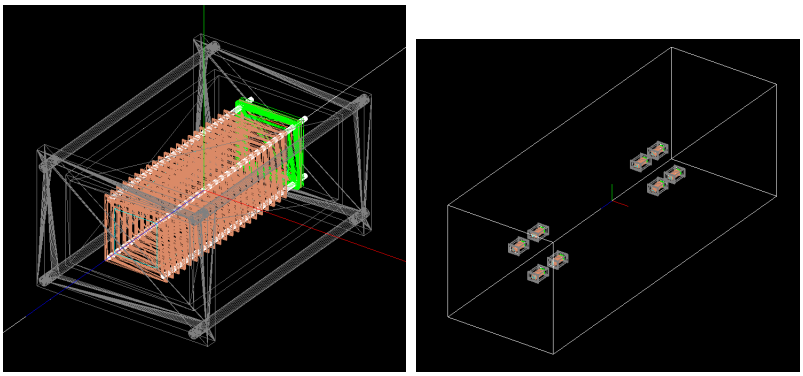

Figure 2: Left: G4 drawing of a single micro-BEAST-TPC. Right: G4 drawing of eight micro-BEAST-TPCs located in the dock space.

Figure 2.1.3-left shows a G4 drawing of a single micro-BEAST-TPC and a G4 drawing of eight micro-BEAST- TPCs located in the dock space (Figure 2.1.3-right).

2.2 Design optimization

2.2.1 TPC position

At this stage, we can not determine the optimum position for the T1 phase. For the phase 2 phase, the TPCs will be located in the dock space. Figures 2.2.1 and 2.2.1 represent two section views: a top view and r-phi views for the backward and forward dock spaces. The rectangular red boxes show the possible TPC positions. Figure 2.2.1 gives also the TPC numbering. The TPCs can be located at different z positions in the backward and forward

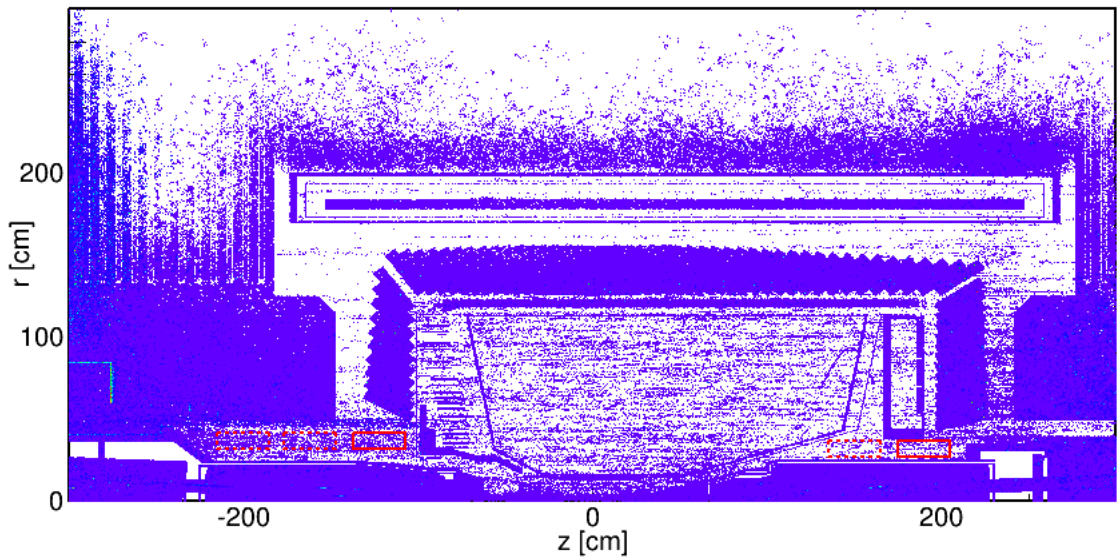

Figure 3: Top view. Distribution for the particle decay points in the radial plane r = $\sqrt{x^2 + y^2}$ versus z-axis.

Table 1: TPC positions in the dock spaces at phase 2.

TPC #	1	2	3	4	5	6	7	8
r [cm]	37	37	37	37	32	32	32	32
z [cm]	-122	-122	-122	-122	190	190	190	190
ϕ [^{o}]	-90	0	90	180	-90	0	90	180

dock spaces: -210 $\leq$ z $\leq$ -105 cm and 155 $\leq$ z $\leq$ 212 cm respectively.

The rates at phase 2 for the different beam-induced backgrounds are shown in Figure 2.2.1 at the locations corresponding to the full red line box of Figure 2.2.1-top-left and Table 1. Figure 2.2.1(-top-right and bottom) show also the rates at alternative locations corresponding to the dashed red line boxes of Figure 2.2.1-top-right and -bottom. The neutron rates amount of 10 % of lower to the total rate. The rates at phase 2 phase will be 100 smaller than the rates at designed luminosity. The rates of reconstructible events that the TPCs can measure will be at least 1000 smaller. So all together at phase 2 phase should be around few 10's Hz at best.

The neutron rates summed for the backward and forward TPCs traversing the TPCs was estimated at phase 2 as function of the neutron kinetic energy, neutron polar and azimuthal angles as seen in Figures 2.2.1-top-row and **??**-top-row and corresponding to the positions of Table 1. The (proton) recoil rates expected was calculated by a Fast Monte Carlo simulation using the two-body kinematic and considering a neutron detection efficiency of 0.1 % in average.

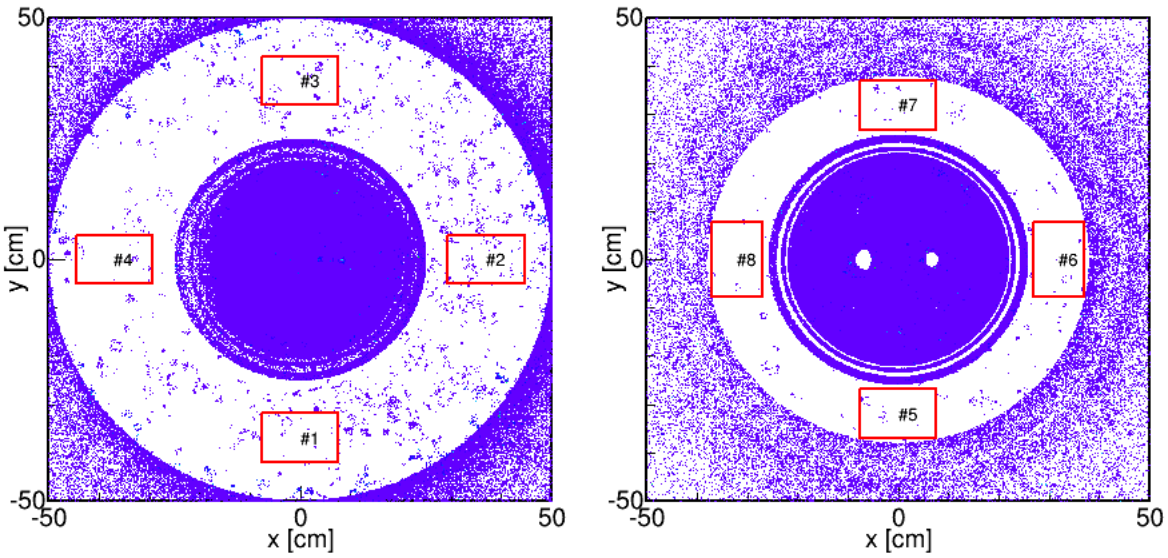

Figure 4: R-phi view. Distribution for the particle decay points in the plane perpendicular to the z-axis. Left: for -210 $\leq$ z $\leq$ -105 cm ie backward dock space. Right: for 155 $\leq$ z $\leq$ 212 cm ie forward dock space.

The dominant beam-induced background are RBB LER and HER and Touschek LER. As function of z the RBB LER and HER rates are more or less constant, while the Touschek LER is decreasing in the backward dock space for negative z because they are further away from the QCS. Although the rates emanating from the tunnel increased for smaller z (labeled far in Figure 2.2.1), the rates will be most likely of the same level than the internal irreducible TPC background.

2.2.2 Gas choice

The gas choice depends of several factors. It should be composed of a light gas-nucleus in order to have a good neutron elastic cross section and also to have recoil with enough energy to produce long enough track that can be detected and still have directionality. In addition, the gas or the gas-mixture should have a drift velocity high enough to clear the chamber volume rapidly but no too high to have a good 3D hit resolution. The drift velocity will be limited in our case by the pixel size 250 μm for the FE-I4 and 400 μm for the FE-I3: v_{drift} x FE-I3/4 time resolution $\leq$ pixel size. For FE-I3: $v_{drift}(E/P) \leq \frac{400\mu m}{25ns} = 16\ \mu m$/ns and for FE-I4: $v_{drift}(E/P) \leq \frac{250\mu m}{25ns} = 10\ \mu m$/ns. Tables 2 and 3 show the maximum values of $v_{drift}(E/P)$ for the lowest D_l at low drift field to keep drift voltage reasonably low and cage field simple for iso-butane and the gas mixture He:CO_2:70:30.

The attachment coefficient should also be low. The gas gain should stable and on the order of 100 for each GEMs. Several gas and gas mixture: iC_4H_{10} (flammable and explosive), Ar:CO_2, He:CO_2, He:CF_4 and He:CH_4 (flammable, but not explosive), have been investigate

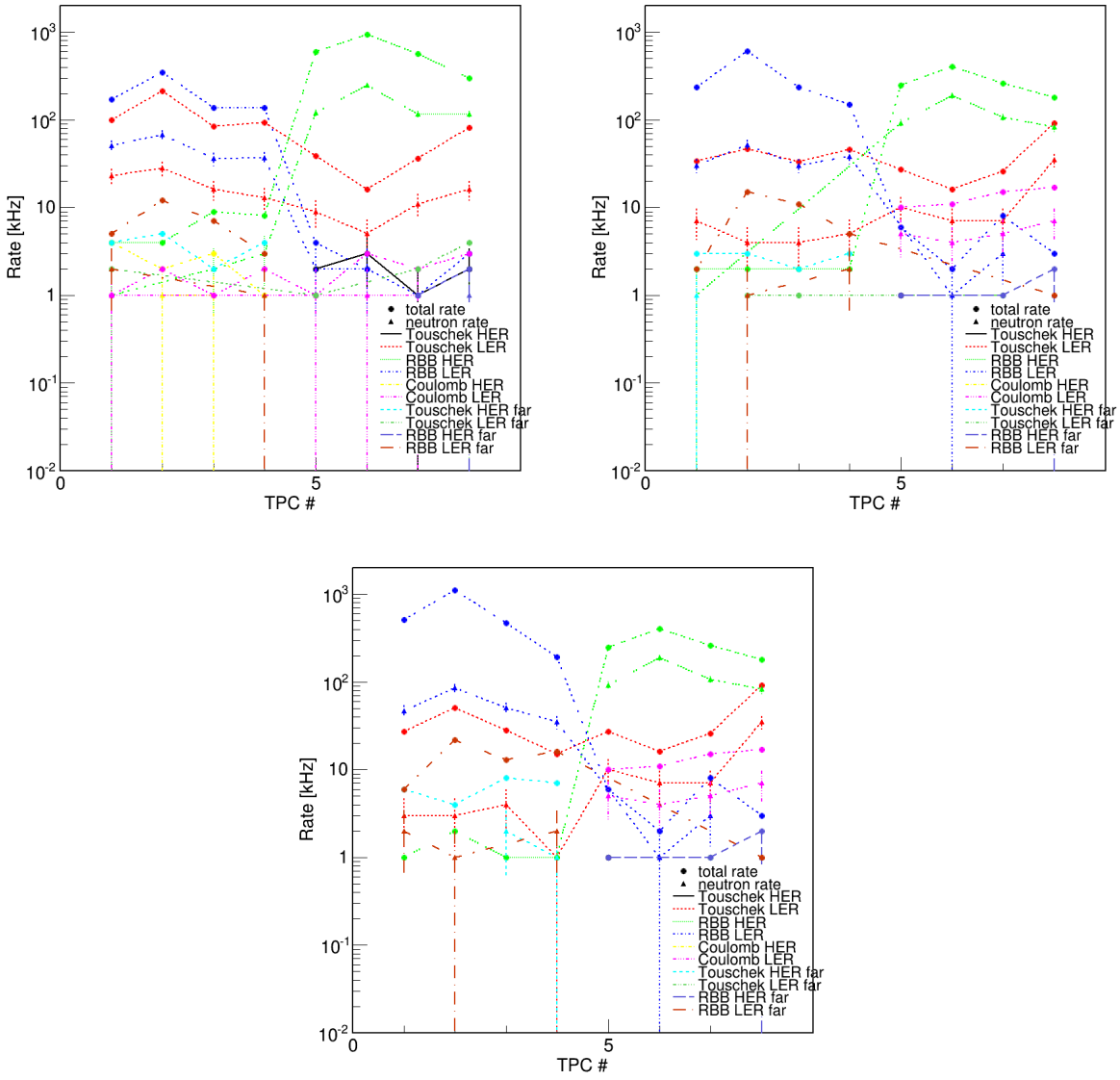

Figure 5: Rates at phase 2 of the different beam-induced backgrounds inside each TPC at different dock space locations. The numbering corresponds to Figure 2.2.1. Left top: rate corresponding to the full red line box in Figure 2.2.1. Right top and bottom: rates corresponding to the dashed red line boxes in Figure 2.2.1. Point symbol total rate. Triangle symbol neutron rate.

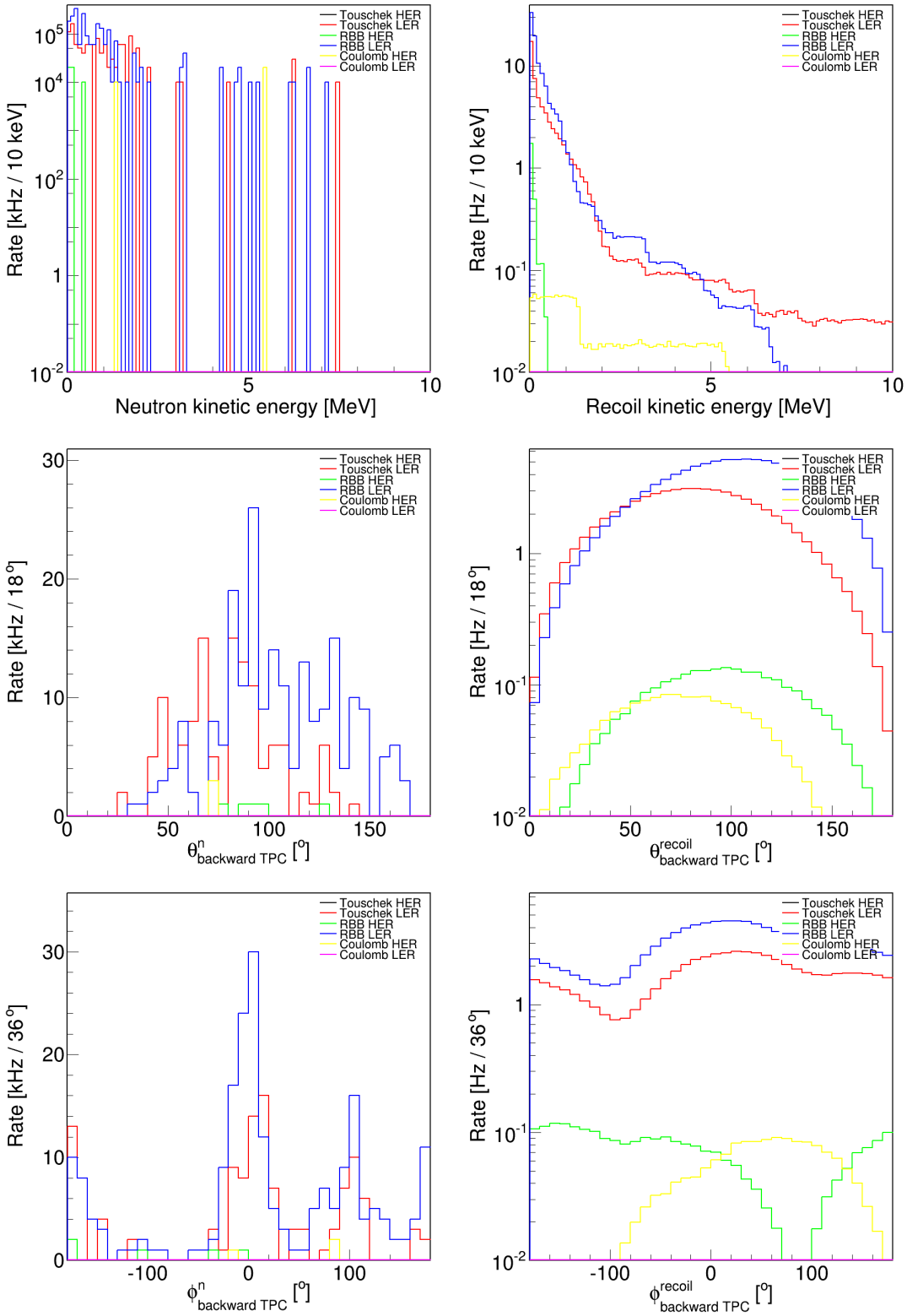

Figure 6: Rates at phase 2 for the beam-induced backgrounds traversing or expected to be measured by the TPCs located in the backward dock-space. Left column: neutron. Right column: proton recoils. Top row: versus kinetic energy. Middle row: versus polar angle. Bottom row: versus azimuthal angle.

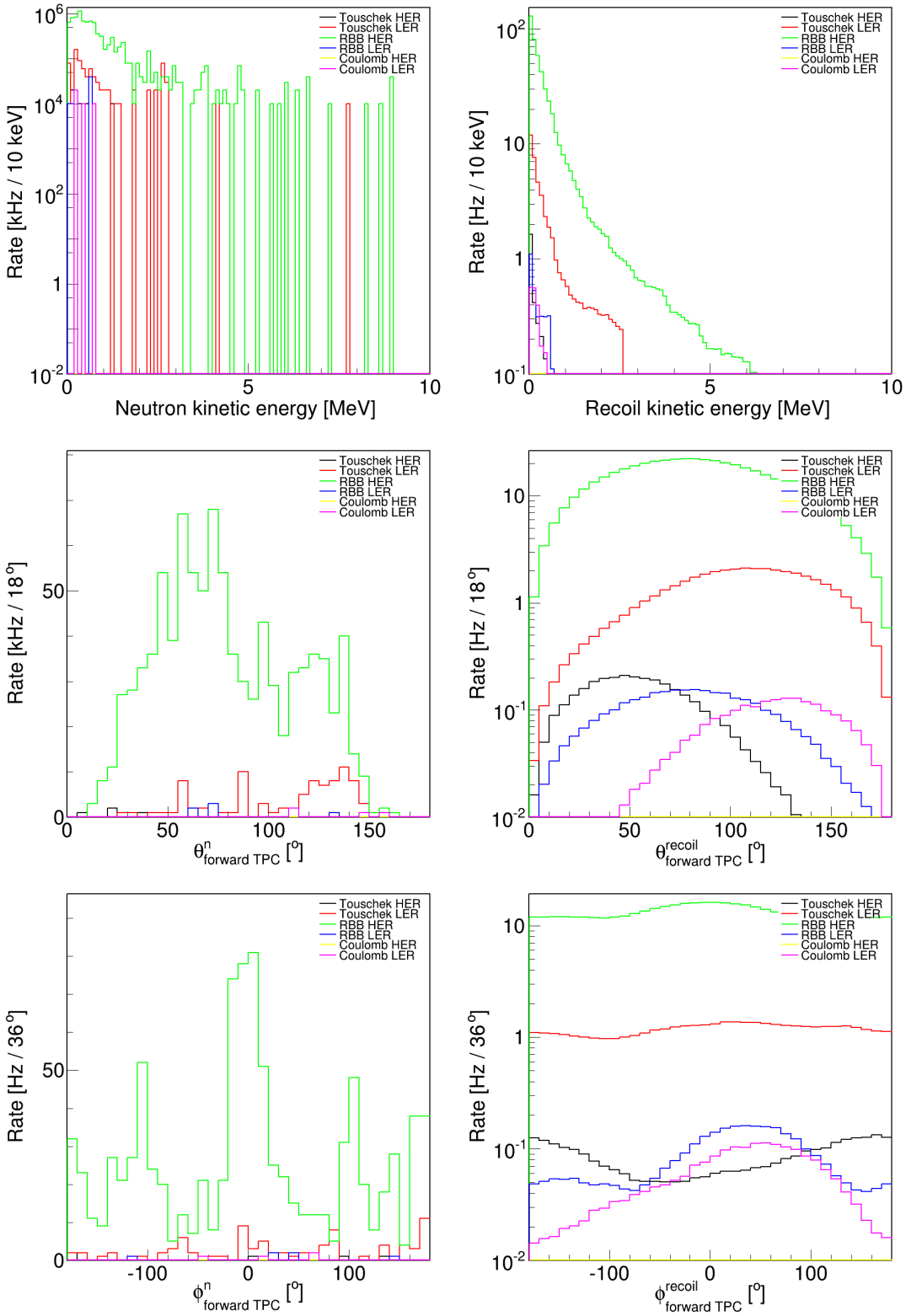

Figure 7: Rates at phase 2 for the beam-induced backgrounds traversing or expected to be measured by the TPCs located in the forward dock-space. Left column: neutron. Right column: proton recoils. Top row: versus kinetic energy. Middle row: versus polar angle. Bottom row: versus azimuthal angle.

Table 2: Iso-butane optimized drift velocity and field.

chip	time resolution [ns]	pixel size [μm]	v_{drift} [μm/ns]	E [kV/cm]	D_t [$\mu m/\sqrt{cm}$]
FE-I3	25	400	16	0.5	130.5
FE-I4	25	250	10	0.3	148

Table 3: He:CO_2:70:30 optimized drift velocity and field.

chip	time resolution [ns]	pixel size [μm]	v_{drift} [μm/ns]	E [kV/cm]	D_t [$\mu m/\sqrt{cm}$]
FE-I3	25	400	16	0.84	124.5
FE-I4	25	250	10	0.53	124.3

with GEANT4 and MAGBOLTZ to determine the neutron probability of interaction per centimeter (Figure 2.2.2), the gas parameters respectively and the mixture composition in case of a gas mixture all at 1 atm. Isobutane has the highest neutron cross section 7 to 9 times higher than He:CO_2:70:30.

Figure 2.2.2 shows gas parameters: the drift velocity and the diffusion (transverse and longitudinal), for the different gas or gas mixture studied, as function of the electric and pressure (with the pressure at 1 atm) ratio. Figure 2.2.2 also illustrates the influence of gases: CH_4, CO_2 and CF_4, which allow depending of the proportion of it compared to Helium to vary the drift velocity for approximately similar diffusions. The evolution of the gas parameters for different proportion of He and CO_2 is shown in Figure 2.2.2. The introduction of CO_2 in higher proportion decreases the drift velocity and also lowered the optimal field needed to be applied in the drift region. The influence of the magnetic has also been studies as an illustration, Figure 2.2.2 shows the magnetic field influence on He:CO_2:70:30 and iso-butane. In general if the magnetic and the electric field are parallel, the influence of the magnetic field has small effect on gases with small drift velocity. If the magnetic and the electric field are not aligned, the drift velocity and the diffusion parameters expression will be more complicate since for example the diffusion will become tensorial and the drift velocity will have components in all direction.

The gas that offers the best trade off between neutron interaction probability, good gas properties and easy to use is He:CO_2:70:30. Iso-butane is the best gas in general but because its dangerosity make its more challenging but KEK has experience with this type of gas.

2.2.3 Field cage

To minimize the internal background due to natural radioactivity and the neutron probability of interaction with the field cage different width of rectangular rings have been studied using COMSOL. Figure 12 shows the electric field streamlines calculated by COMSOL. Figure 2.2.3

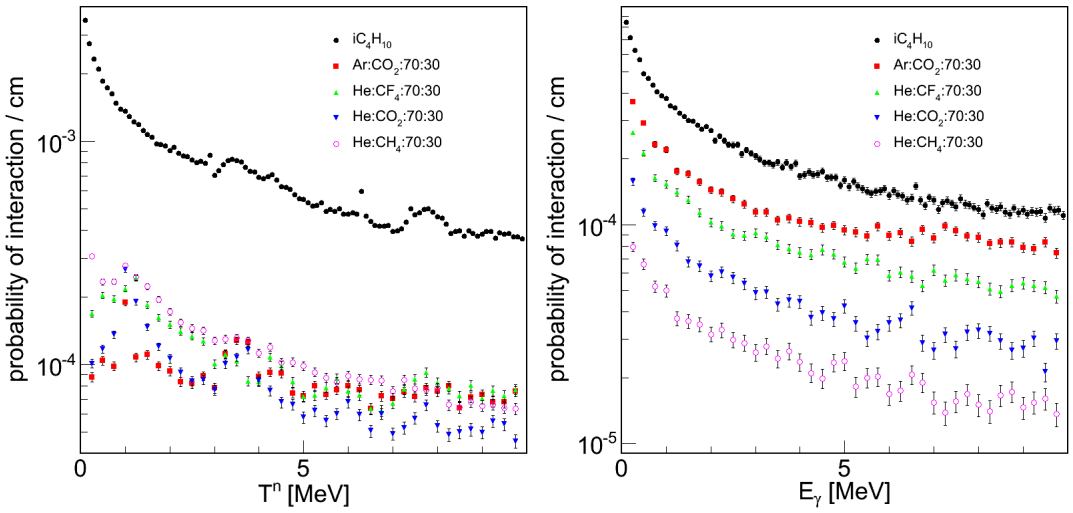

Figure 8: Interaction probability per centimeter as function of kinetic energy for various gas and gas mixtures. Left: neutron. Right: photons.

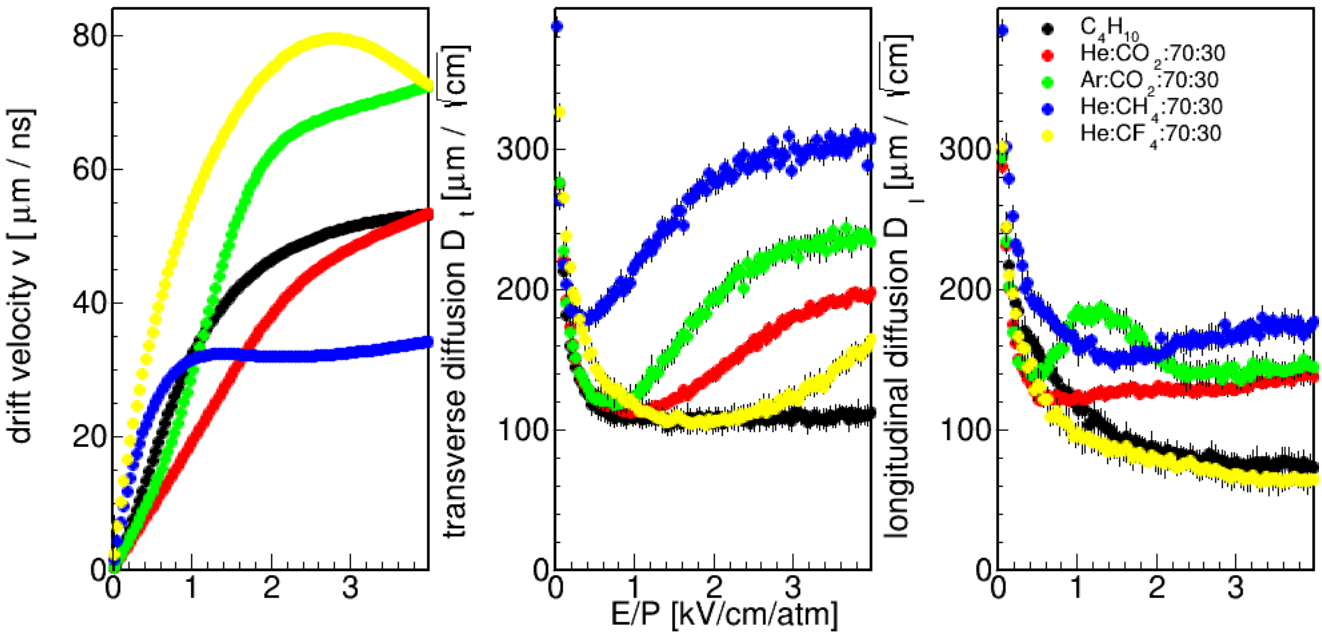

Figure 9: Gas parameters calculated by MAGBOLTZ as function of electric field and pressure (P = 1 atm) ratio for the different gas or gas mixture candidates studied.

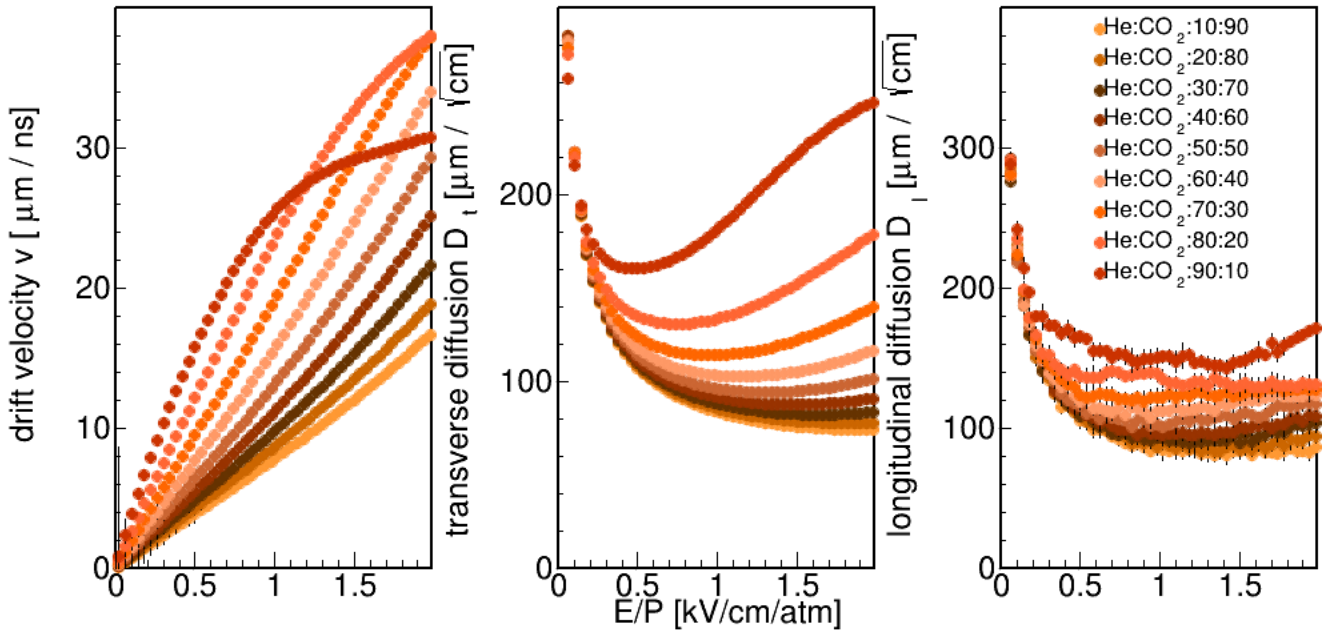

Figure 10: Gas parameters calculated by MAGBOLTZ as function of electric field and pressure (P = 1 atm) ratio for the different percentage of Helium and carbon di-oxygen.

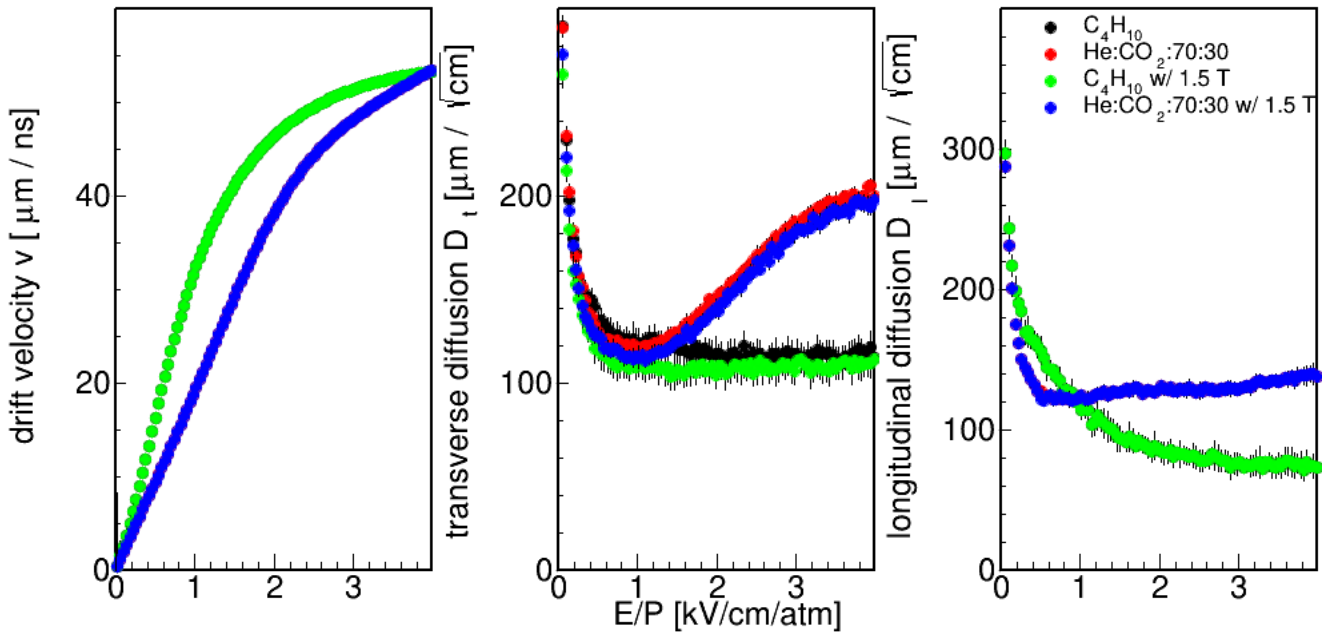

Figure 11: Gas parameters calculated by MAGBOLTZ as function of electric field and pressure (P = 1 atm) ratio for the He:CO_2:70:30 and iso-butane without and with 1.5 T magnetic field.

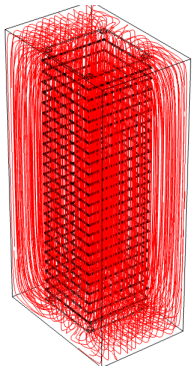

Figure 12: Electric field streamlines calculated by COMSOL.

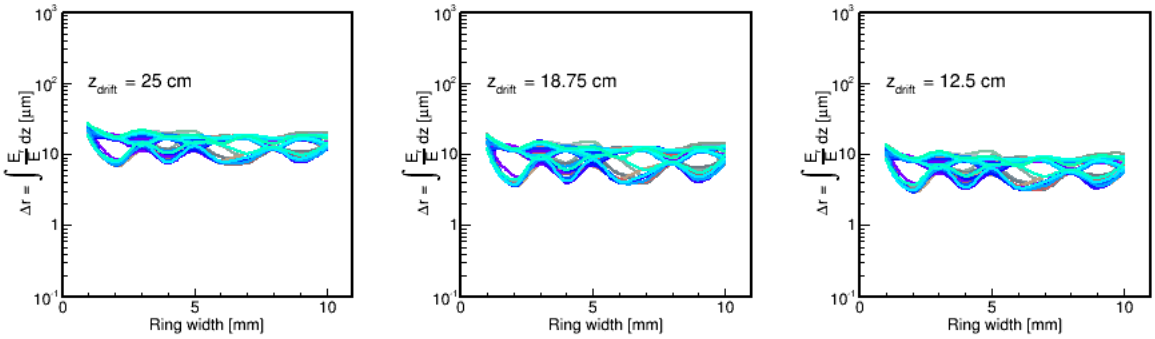

Figure 13: Radial distance an electron drifts from different drift distance to the bottom of the field cage. Left: from top to bottom. Middle: from 18.75 cm to bottom. Right: from 12.5 cm to bottom.

shows the radial diffusion as function of the ring width at different transverse positions. The radial distance an electron can drift is below 40 μm ie below the pixel height (50 μm). A mm width can be used for the field cage.

2.2.4 Gain choice

To achieve the highest possible detection of the primary ionization, Gas-Electron-Multipliers (GEMs) are used to amplify the signal. The GEMs have very good rate capability and intrinsic ion feedback suppression. GEMs are also gate-less and can operate continuously. Each GEM has a gain of the order of 100 in a gas chosen adequalety. The gain has to be adapted to the amount of ionization, that the recoil we want to measure, losses. The electronic energy loss to the gas electron per centimeter can be calculated by using SRIM as illustrated in Figure 2.2.4. From this curve, an average number of electrons that can reach a GEM hole can be calculated.

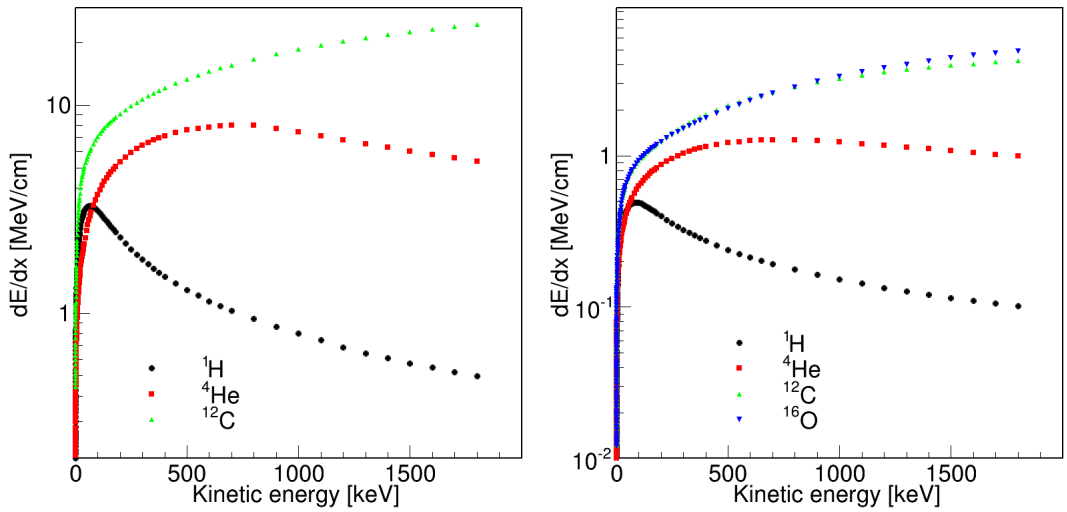

Figure 14: SRIM calculation of electronic energy loss to the gas electron per centimeter versus recoil kinetic energy. Left: Black point H. Red square He, Green triangle C in C_4H_{10} at 1 atm. Right: Black point H. Red square He, Green triangle C and Blue triangle down O in He:CO_2:70:30 at 1 atm.

Table 4: Average electron number per pixel and optimal gain for He:CO_2:70:30 and C_4H_{10} at 1 atm.

gas	He in He:CO_2:70:30	H in C_4H_{10}
electron number per pixel	171	1294
optimal gain	2800	400

Since roughly a pixel is in front of two GEM holes, we can deduce the optimal gain necessary to be above the pixel threshold. A figure-of-merit, Figure 2.2.4, can be constructed that takes into account pressure, diffusion, pixel threshold and range. Table 4 summarizes the results.

2.2.5 Pixel chip choice

There are two version of the pixel chip: FE-I3 and FE-I4. A short description can be find below.

- FE-I3
  - chip size 0.84 cm x 0.76 cm
  - pixel size 50 μm x 400 μm
  - 18 column x 160 row

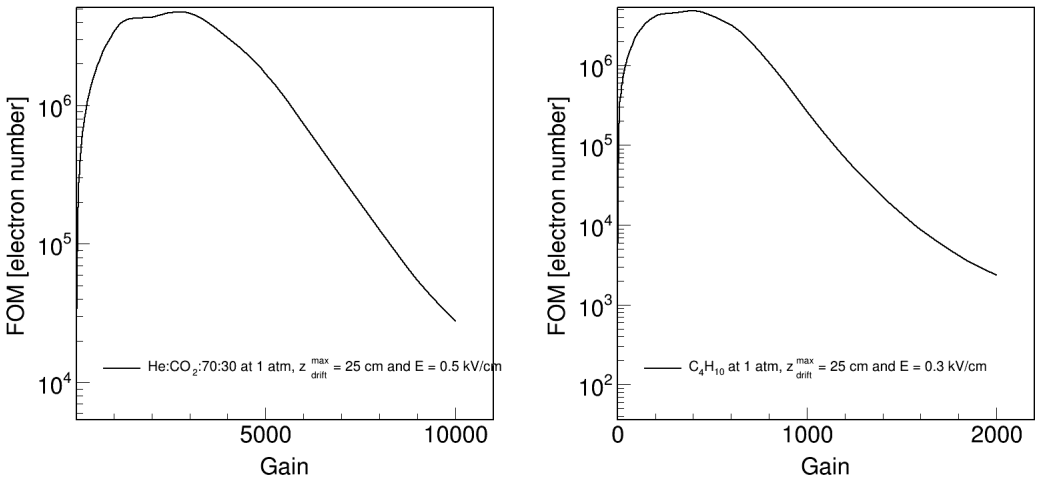

Figure 15: Gain figure-of-merit for 25 cm drift distance, 1 atm and 200 μm pixel size. Left: for He in He:CO_2:70:30. Right: for H in C_4H_{10}.

  - 400 ns time range with 16 graduation
  - threshold 2215 electrons
  - 100k e^- charge range with 128 graduation

- FE-I4
  - chip size 2 cm x 1.68 cm
  - pixel size 50 μm x 250 μm
  - 80 column x 336 row
  - 1600 ns time range with 64 graduation
  - threshold 1384 electrons
  - 100k e^- charge range with 16 graduation

Table 4 can be converted into Table 5 which highlights the ionization energy each (FE-I4) pixel should record for He:CO_2:70:30 or/and C_4H_{10} (both at 1 atm). Even if the FE-I4 has much less charge graduation than the FE-I3 if the GEMs gain is properly chosen, the FE-I4 can reach an intrasic energy resolution of 290 eV and 1.38 keV tuned respectively for He in He:CO_2:70:30 and H in C_4H_{10}. The GEM and gas intrasic energy resolutions, roughly 20 % for both, should be added in quadrature ie total $\Delta E = 1.33$ and 6.4 keV respectively for He in He:CO_2:70:30 and H in C_4H_{10}.

If the TPC is correctly optimized the angular resolution should be dominated by the straggling as illustrated in Figures 2.2.6 and 2.2.5

Table 5: Work function and mean ionization energy recorded per FE-I4 pixel for He:CO_2:70:30 and C_4H_{10} at 1 atm.

gas	He in He:CO_2:70:30	H in C_4H_{10}
Work function [eV/ion-electron-pair]	35.075	23.4
ionization energy per pixel [keV]	4.6	22

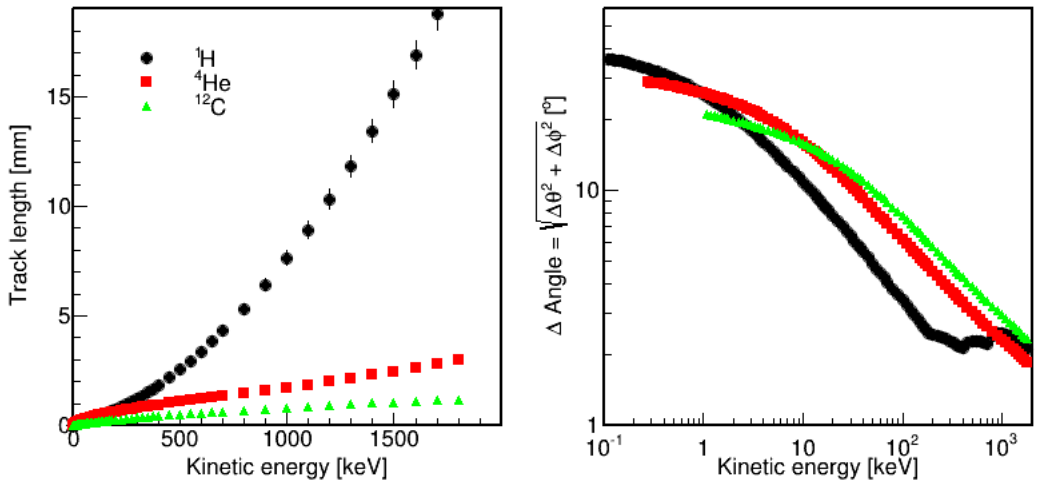

Figure 16: Left: track length versus recoil kinetic energy in C_4H_{10}. Right: angular resolution due the longitudinal and transverse straggling versus recoil kinetic energy in C_4H_{10}.

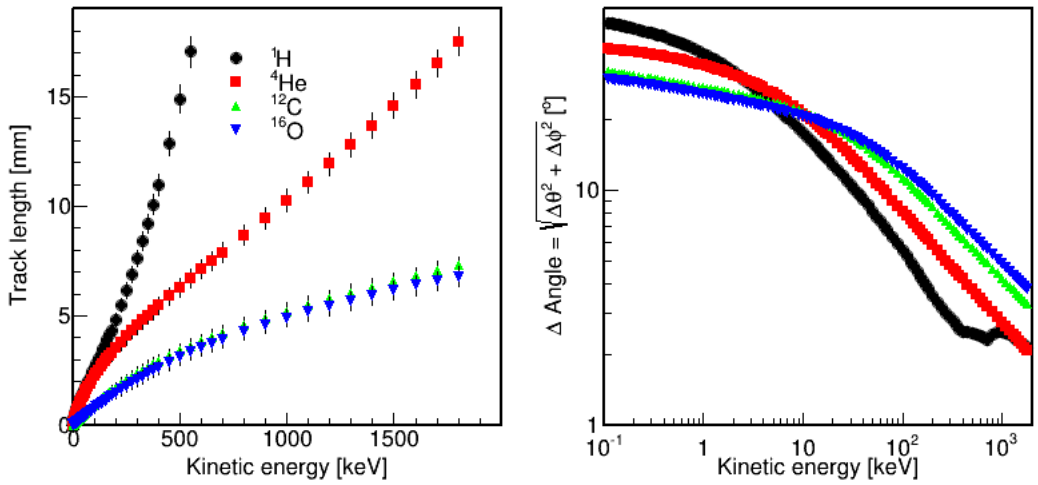

Figure 17: Left: track length versus recoil kinetic energy in He:CO_2:70:30. Right: angular resolution due the longitudinal and transverse straggling versus recoil kinetic energy in He:CO_2:70:30.

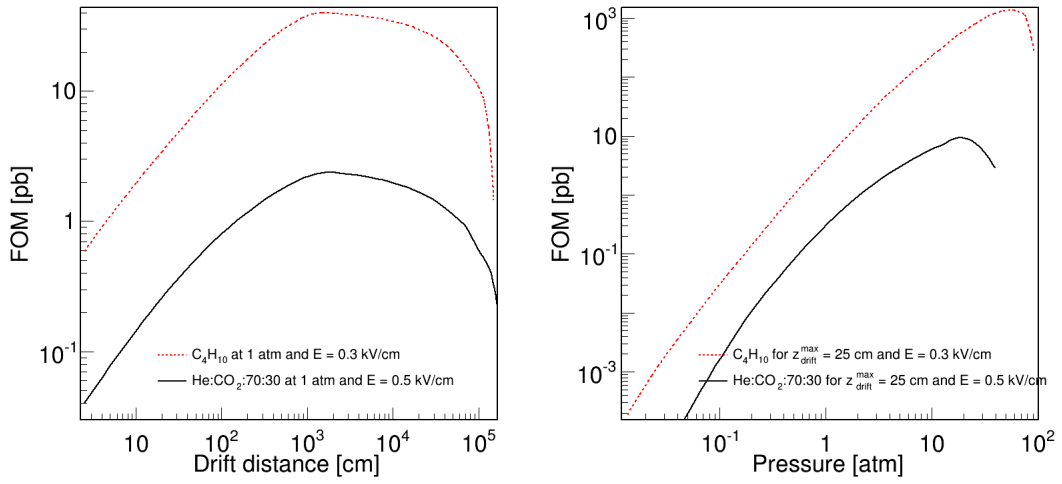

Figure 18: Left: drift distance figure-of-merit. Right: pressure figure-of-merit.

2.2.6 Pressure and drift length choices

The pressures as well as the drift length can be optimized by determining a figure-of-merit. The pressure and the drift length figure-of-merits take into account the recoil energy spectrum due to the neutron and the directionality by considering that the diffusion effect is dominating the directionality: $L > 6.\sigma_{diffusion}(z)$ ie HT is not taken into account.

The fact that the optimum drift distance is well above 25 cm can be explained by the increase of the target volume and the long tail in the recoil energy spectrum see Figure 2.2.1-bottom-left.

The iso-butane start to be liquid above 2 atm but the He:CO_2:70:30 can operate in principal at higher pressure. It should be noted that He:CO_2:70:30 $\sim$ 8 atm has the same figure-of-merit than iso-butane at 1 atm. For He:CO_2:70:30 at 8 atm, the optimum gain is 90 implying that one GEM might be enough.

2.3 Rates and Detection efficiency

Several conditions are imposed on the track to ensure that the projection of the track, with a length L, on the two-dimensionally segmented pixel chip readout plane can be exploited to extract the directionality:

- L $> 6\ \sigma_{xy}$ where σ_{xy} is the transverse diffusion
- L $> 3 \times$ GEM holes spacing
- $\Delta E_{HT} > 6\ .\ \Delta E$(E) where ΔE_{HT} is the difference in energy between the head (E_H) and the tale (E_T) and ΔE(E) the energy resolution

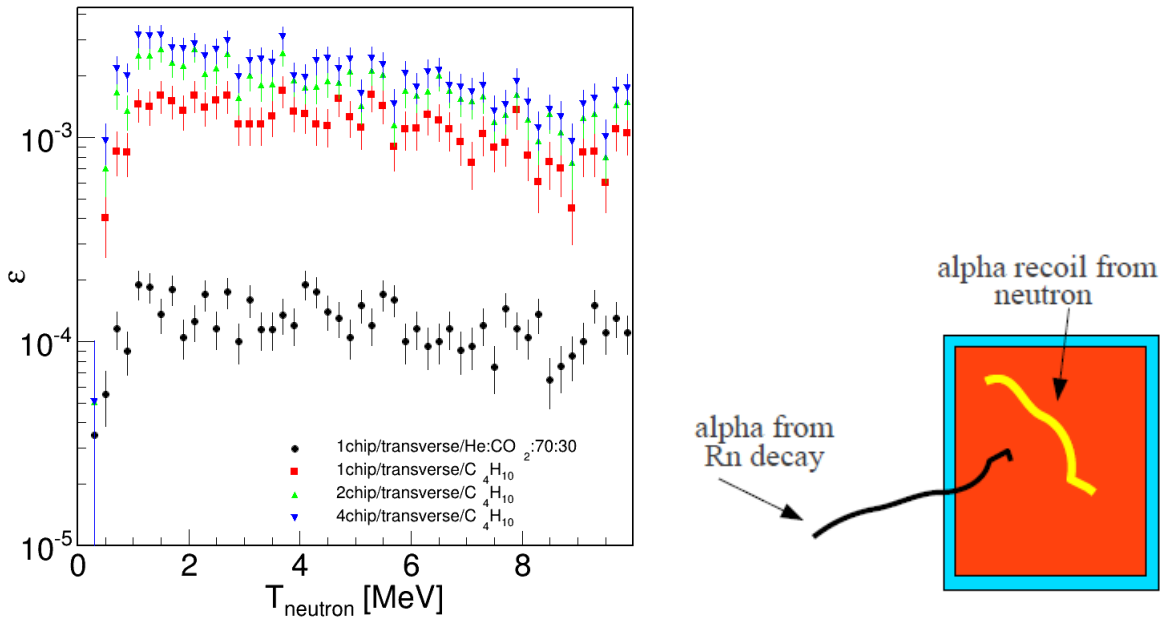

Figure 19: Left: Neutron detection efficiency as function of the neutron kinetic energy and number of pixel chip used. Right: edge cut drawing. Edge represented by the blue aera.

A so-called edge cut (Figure-right 19) is also applied to remove alpha-particle coming from natural radiation contained in the detector material and which are located outside of the sensitive volume. This background is critical particularly for He:CO_2:70:30 gas-mixture, since one cannot distinguish an alpha-particle recoiling due to a neutron scattering elastically on it to an alpha-particle coming from a Radon decay chain for example. The current irreducible background rate in the sensitive volume after an edge cut with the micro-DCube prototype, which used the FE-I3 pixel chip, is around 0.2 per minute. So if one considers that the irreducible background will scale with the surface then 0.2 x A(4 FE-I4) x A(1 FE-I3) ie 4.2 per minute ie roughly 0.1 Hz for the micro-BEAST-TPCs. The irreducible background is represented by a black line at 0.1 Hz in Figure 20 or by a line at 0.044 Hz (0.1 Hz x 8 TPC / 18^o) in the TPC angular plot rates: Figures 21, 22 and 23. Figure 20 shows the neutron rates with recoil exploitable directionality per TPC compared to the total rates in the TPCs.

Figures 21, 22 and 23 show the angular neutron rates for all TPCs combined with recoil exploitable directionality for the gas-mixture He:CO_2:70:30 and iso-butane both at 1 atm for the different beam-induced backgrounds.

The neutron detection efficiency as function of the neutron kinetic energy for iso-butane and the gas-mixture He:CO_2:70:30 (both 1 atm) for one, two and four FE-I4 pixel chips, Figure-left 19-left. Between one chip with gas-mixture He:CO_2:70:30 at 1 atm and four chips with iso-butane at 1 atm there is a factor ~ 8 improvement.

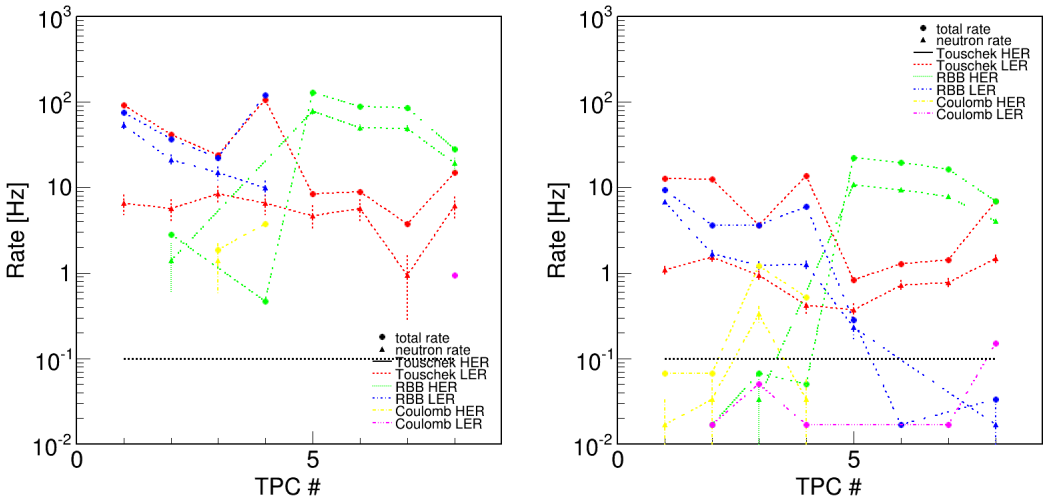

Figure 20: Rate at phase 2-phase recorded by four FE-I4 pixel chips in each TPC for the different beam-induced backgrounds. Left for C_4H_{10} at 1 atm. Right for He:CO_2:70:30 at 1 atm. The neutron rates correspond to the rate of recoil with directionality and edge cut. The total rates include all particles seen all hits recorded by the pixel chips. The black line represents the irreducible background expected.

The neutron detection efficiency is also compared to the electron/positron and muons detection efficiencies in Figure 24.

2.3.1 Commissioning Detector Dose Monitor

2.3.2 Commissioning Detector: PXD group plans

2.3.3 Commissioning Detector Luminosity Monitoring Device

2.3.4 Commissioning Detector micro-TPCs

References

[1] T. Kim, M. Freytsis, J. Button-Shafer, J. Kadyk, S. E. Vahsen and W. A. Wenzel, "Readout Of TPC Tracking Chambers With GEMs And Pixel Chip", Nucl. Instrum. Meth. **A589** (2008), 173-184

[2] R. Cizeron, A. Durand, T.L. Geld, V. Lepeltier, B. Meadows, Michael T. Ronan, S. Sen, A. Valassi, G. Wormser, "A Mini - TPC for SLAC B factory commissioning", Nucl. Instrum. Meth. **A419** (1998), 525-531

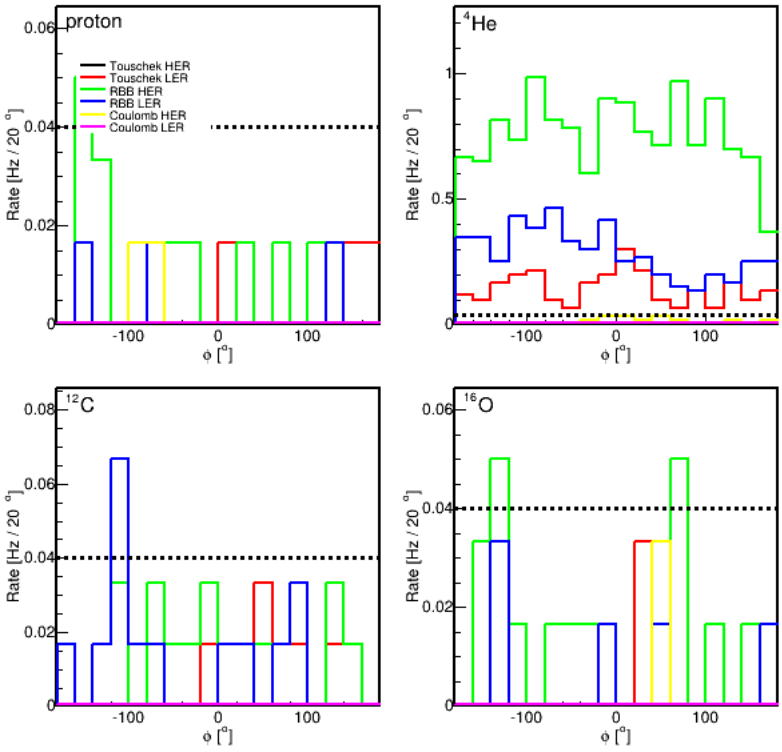

Figure 21: Rate of recoils (with directionality) versus azimuthal angle in He:CO_2:70:30 at 1 atm for the different beam-induced backgrounds at phase 2 and for all TPCs combined. Top-left: proton knock off from the detector materials. Top-right: He recoil. Bottom-left: carbon recoil. Bottom-right: oxygen recoil.

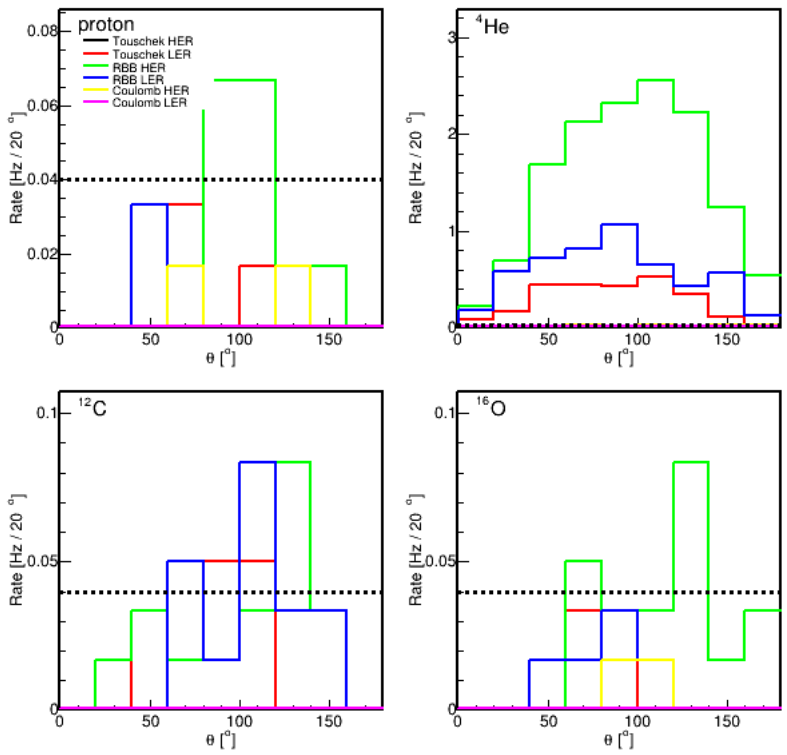

Figure 22: Rate of recoils (with directionality) versus polar angle in He:CO_2:70:30 at 1 atm for the different beam-induced backgrounds at phase 2 and for all TPCs combined. Top-left: proton knock off from the detector materials. Top-right: He recoil. Bottom-left: carbon recoil. Bottom-right: oxygen recoil.

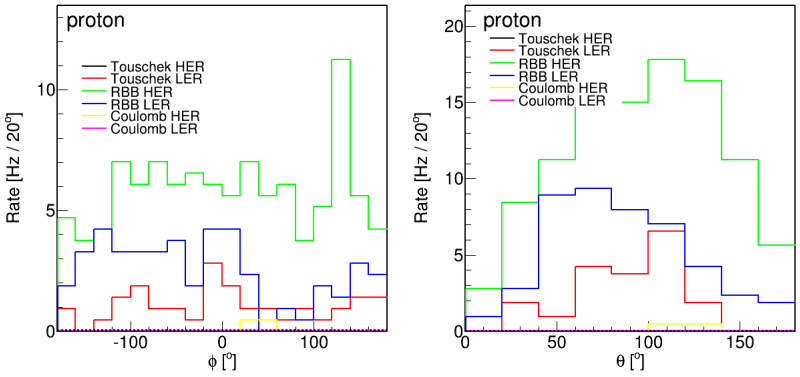

Figure 23: Rate of proton recoils (with directionality) in C_4H_{10} at 1 atm for the different beam-induced backgrounds at phase 2 and for all TPCs combined. Left: rate versus azimuthal angle. Right: rate versus polar angle.

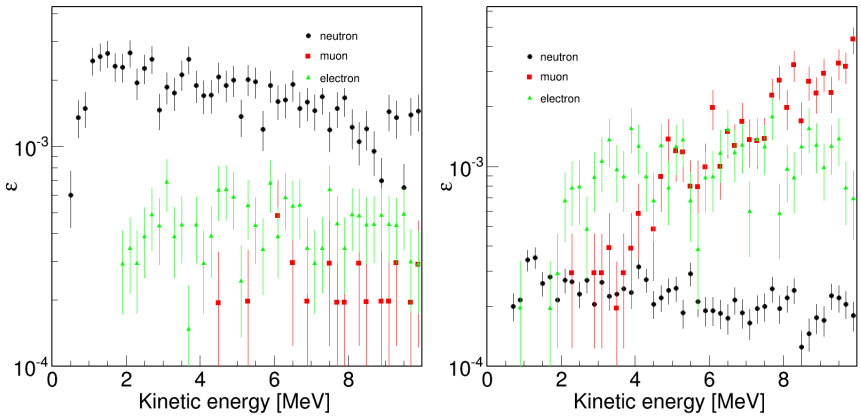

Figure 24: Detection efficiency of neutron, electron/positron and muons as function of the kinetic energy and number of pixel chip used. Left: for He:CO_2:70:30 at 1 atm. Right: for C_4H_{10} at 1 atm.

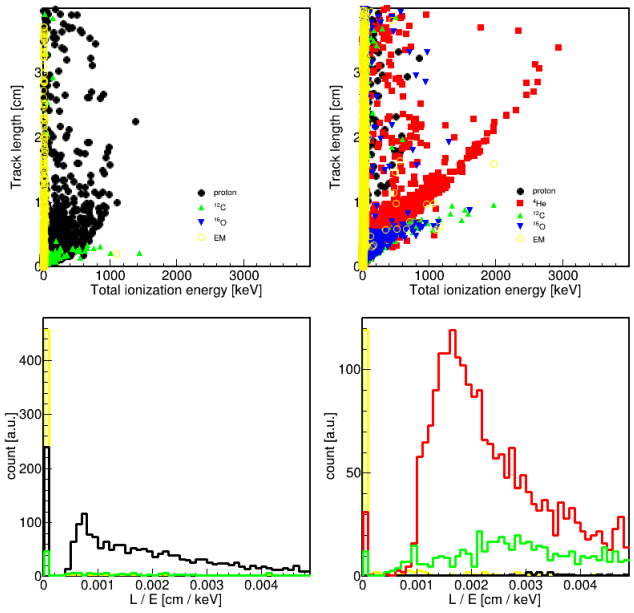

Figure 25: Top row: track length versus total ionization energy. Bottom row: L / E.

[3] K. Miuchi et al., "Performance of a micro-TPC for a time-resolved neutron PSD", Nucl. Instrum. Meth. **A517** (2003), 219-225

[4] J. Yamaoka, H. Feng, M. Garcia-Sciveres, I. Jaegle, J. Kadyk, Y. Nguyen, M. Rosen, S. Ross, T. Thorpe, S. Vahsen, "Application of Time Projection Chambers with GEMs and Pixels to WIMP Searches and Fast Neutron Detection", TIPP2011, submitted to Elsevier Physics Procedia (2011)

[5] S. E. Vahsen, H. Feng, M. Garcia-Sciveres, I. Jaegle, J. Kadyk, Y. Nguyen, M. Rosen, S. Ross, T. Thorpe, J. Yamaoka,"The Directional Dark Matter Detector", arXiv:1110.3401v1 (2011)